Comparative Analysis Between Robust SMC & Conventional PI Controllers Used in WECS Based on DFIG

Mohammed Fdaili*‡, Ahmed Essadki*, Tamou Nasser**

* Electrical Engineering Department of Higher Normal School of Technical Education (ENSET) Mohammed V University, Rabat-Morocco.

** Electrical Engineering Department of National School of Computer Science and Systems Analysis (ENSIAS) Mohammed V University, Rabat-Morocco.

(mohamed.fdaili@um5s.net.ma, ahmed.essadki1@gmail.com, tnasser@ensias.ma)

‡ Corresponding Author; Mohammed Fdaili, Tel: +212 660 995 478,

mohamed.fdaili@um5s.net.ma

Received: 02.05.2017 Accepted:25.07.2017

Abstract- In this paper, a direct and indirect stator powers control schemes based on Proportional-Integral (PI) and sliding mode control (SMC) strategies of a doubly fed induction generator (DFIG) used in wind energy conversion system (WECS) are presented. The classical PI controllers present many limitations due to the nonlinearity of the DFIG model. Therefore, in order to improve the system performances, a new algorithm that combines the nonlinear sliding mode control approach and field orientation scheme applied to the DFIG converters is developed. The MPPT and the pitch angle algorithm control are used to extract the maximum power and to protect the system of a wind turbine from overloading, respectively. The performances of the proposed controllers system were tested, analyzed and compared in dynamic and steady state by using Matlab/Simulink.

Keywords Wind energy conversion system, Sliding mode control, PI controller, Doubly-fed induction generator, MPPT algorithm control, Pitch angle.

1. Introduction

The global energy consumption has seen an enormous increase in recent years due to the massive industrial development. This consumption tends to increase more and more [1]. In [2], China is a remarkable case of this consumption increase. The risk of fossil fuel scarcity and its effect on climate change; denote again the importance of renewable energies, particularly the wind turbine.

During the last years, the DFIG has received an enormous attention as one of the most preferred technologies used in variable speed wind turbine system (WTS) [1].This type of machines offers a lot of benefits, such as the potential to control torque, the reduction of inverter cost [3] and increase the efficient extraction of available energy.

A vector control based on the orientation of the stator field is applied to independently control the powers transmitted between the electrical grid and the DFIG's stator side [4]. Thus, the DFIG model becomes simple and less difficult, so the classical PI controllers can be used. The direct and indirect vector control (DVC and IVC, respectively) are based on this type of controllers to regulate the stator powers. However, this technique of control is directly dependent on parameters of DFIG, uses one (DVC) or multiples (IVC) loops and also it requires much regulation effort to assure the stability of the overall system. [3].

In this last years, a lot of control schemes have been elaborated and employed to achieve high performances of the controlled system. These control techniques are based on the field oriented control schemes (FOC). A classical PI, LQG (Linear quadratic Gaussian), polynomial RST and DTC control schemes of DFIG integrated into a wind energy

system are employed in many research papers [5, 6, 7]. In [8, 16], the authors propose a PI control strategy for the rotor side converter (RSC) and the grid side converter (GSC). These controllers present suitable performances in the dynamic and steady state. Nevertheless, this type of controllers suffers from many limitations, such as the machine parameter variations and the nonlinearity of the DFIG model.

The most parts of the wind energy conversion system are not linear (turbine, DFIG); therefore, the classical PI controllers are not efficient in this case. In order to suppress the limitations of the PI controllers (DVC and IVC), sliding mode control has been presented. In the conventional SMC, stator powers of DFIG (active and reactive) can be indirectly controlled by using two sliding surfaces. Nevertheless, one problem limits the use of this controller, such as chattering phenomenon [9]. A lot of solutions were proposed to minimize or avoid this drawback. In many research papers published on SMC, this undesirable phenomenon can be solved by combining fuzzy logic and SMC [10] or replacing the "sign" function by the saturation one [11], however, the robustness of the SMC is improved. The objective of the MPPT technique is to improve the effectiveness of WTS by extracting the maximum power from the available kinetic energy; on the other hand, the pitch angle is used to protect the WTS from overloading in the case of high wind speed.

The rest of the paper is organized as follows: section 2 presents the modeling of the turbine system. The control schemes of MPPT and pitch angle are presented in section 3. The DFIG model based on the stator field oriented control scheme (SFOC) is given in section 4. Then, the vector control (DVC and IVC) strategies are applied in section 5. Section 6 is devoted to controlling the stator powers of the DFIG by using the SMC control scheme. The Simulation results are presented and discussed in section 7, then we finished by the conclusion.

2. Modeling of the Turbine

An Aerogenerator, commonly called wind turbine is a device used to convert the kinetic energy of wind into mechanical power. This wind conversion system is presented in Fig.1.

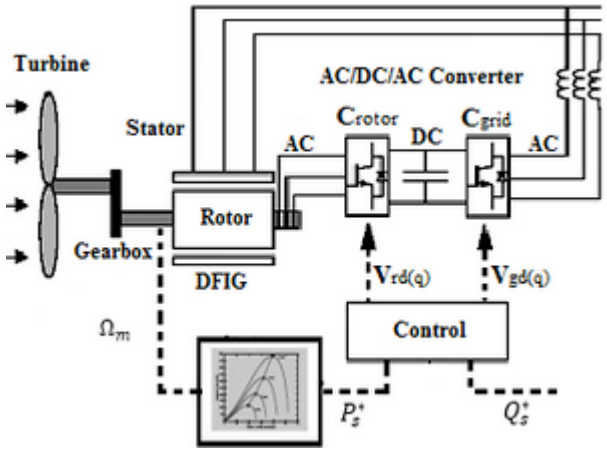

Fig. 1. Wind energy conversion system (WECS)

The aerodynamic power captured on the slow shaft of the turbine can write as [4, 12]:

$$P_{aer} = \frac{1}{2} C_p(\lambda,\beta).\rho.S.V^3 \quad (1)$$

ρ, S and V represent respectively the density of air, the surface swept by the blades and the wind speed.

In our case, the variations of $C_p(\lambda,\beta)$ are modeled by the following exponential approximation [14, 15]:

$$C_p(\lambda,\beta) = A_1\left[\frac{A_2}{\lambda_i} - A_3.\beta - A_4\right]e^{-A_5\left(\frac{1}{\lambda i}\right)} + A_6.\lambda \quad (2)$$

Where: $A_1 = 0.5109$, $A_2 = 116$, $A_3 = 0.4$, $A_4 = 5$, $A_5 = 21$, $A_6 = 0.0068$ and:

$$\frac{1}{\lambda_i} = \frac{1}{\lambda + 0.008\beta} - \frac{0.0035}{\beta^3 + 1} \quad (3)$$

The tip speed ratio (λ) can be expressed as the ratio between the speed of the blades and the wind speed as presented in [13, 15, 18, 12]:

$$\lambda = \frac{R.\Omega_{tur}}{V} \quad (4)$$

Where R and V represent respectively the turbine radius and wind speed.

Figure 2 represents the power coefficient curves as a function of λ for different values of β. The maximum value of C_p ($C_{p-\max}$=0.4745) is achieved for λ_{cp-opt}=8.16.

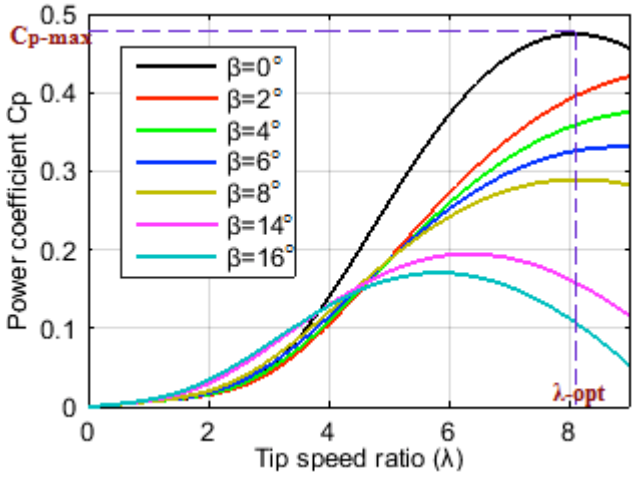

Fig. 2. Power coefficient as a function of λ.

For an ideal gearbox, the aerodynamic torque can be defined as:

$$C_{aer} = G.C_g \quad (5)$$

Where G and C_g represent respectively the gearbox gain and the torque of the fast shaft.

The fundamental equation of the dynamic makes it possible to determine the development of the rotational speed

from the mechanical torque C_{mec} available on the rotor of the machine:

$$J\frac{d\Omega_m}{dt} = C_{mec} \quad (6)$$

With J represents the moment of inertia.

3. Control Strategies of the Turbine

3.1. MPPT (Maximum Power Point Tracking) with control of speed

The DFIG and its converter are supposed ideal, so the developed electromagnetic torque is permanently equal to its reference value [16]:

$$C_{em} = C_{em}^* \quad (7)$$

By imposing the C_{em}^* as given in the following relation [16, 17], the mechanical speed remains equal to its reference value whatever the wind speed (see Fig.3):

$$C_{em}^* = \left(K_p + \frac{K_i}{s}\right).\left(\Omega_m^* - \Omega_m\right) \quad (8)$$

Where K_p and K_i represent the parameters of PI controller, s is Laplace's index.

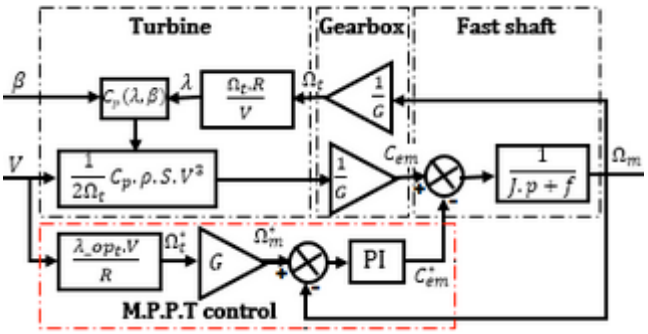

Fig. 3. MPPT strategy with control of speed

From Eq. (4) the reference mechanical speed of the fast shaft corresponds to the optimum value of the tip-speed ratio λ_{cp-opt} can be given as:

$$\Omega_m^* = \frac{V.\lambda_{cp-opt}.G}{R} \quad (9)$$

3.2. Pitch angle control

The control strategy of the pitch angle is used to protect the WTS from overloading in the case of high wind speed, and also for providing the continuity of generated electrical energy by limiting the mechanical power to its rated value. When the wind speed is increasing, the values of β are increased to reduce the values of power coefficient and, consequently, to limit the mechanical power to its nominal value [17]. The error signal between the rated power (7.5 KW) and the measured one is sent to PI controller to produce at its output the reference pitch angle β_{ref}, as shown in Fig.4.

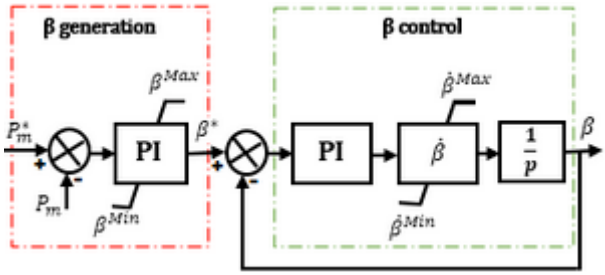

Fig. 4. Pitch angle control system

Figure 5 and Fig.6 represent respectively the profile of wind speed variations and the DFIG's mechanical speed obtained by using the MPPT with control of speed. The measured mechanical speed tracks almost perfectly its reference as we can see in the Fig.6.

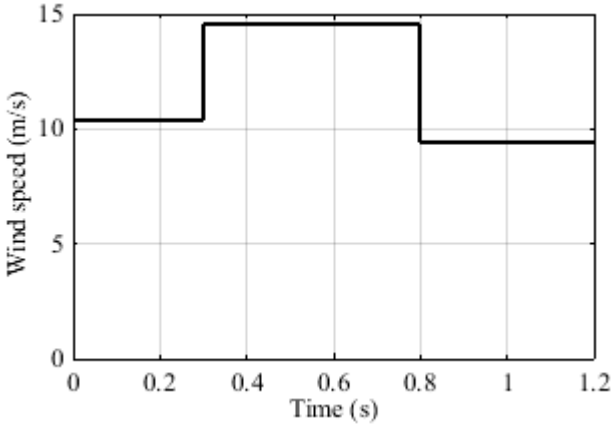

Fig. 5. Wind speed profile

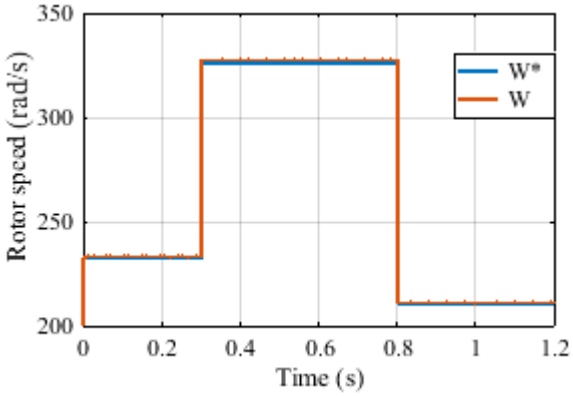

Fig. 6. Mechanical rotor speed of the DFIG

From Fig.8, it can be remarked that the generated values of pitch angle increase, which decrease the $C_p(\lambda,\beta)$ values, when the value of wind speed exceeds the rated one (12.48 m/s). In this case, the regulation intervenes and the pitch angle varies between 0 ° and 20 ° in order to limit the mechanical power appearing on the fast shaft to its nominal value 7.5 KW (see Fig.7), which protect the WTS from overloading.

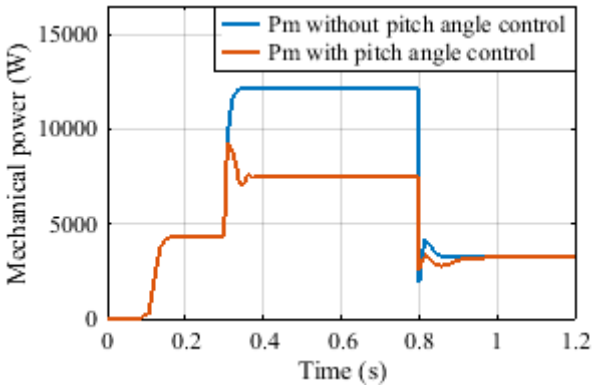

Fig. 7. Mechanical power limitation

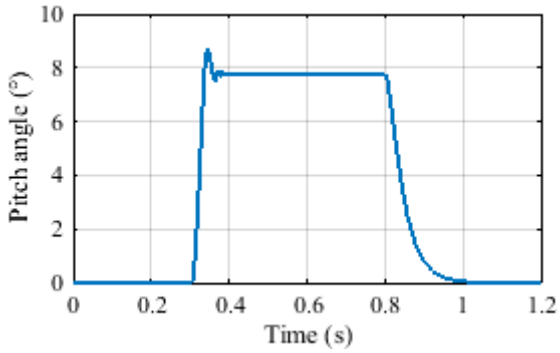

Fig. 8. Pitch angle variations

4. DFIG Modeling

The Park model of the DFIG is extensively used in the literature, as given for example in [17, 19]. The following electrical equations describe the DFIG model in the synchronous d-q Park's reference system rotating at w_s speed [18]:

$$\begin{cases} V_{sd} = R_s.I_{sd} + \dfrac{d\varphi_{sd}}{dt} - \omega_s.\varphi_{sq} \\ V_{sq} = R_s.I_{sq} + \dfrac{d\varphi_{sq}}{dt} + \omega_s.\varphi_{sd} \\ V_{rd} = R_r.I_{rd} + \dfrac{d\varphi_{rd}}{dt} - \omega_r.\varphi_{rq} \\ V_{rq} = R_r.I_{rq} + \dfrac{d\varphi_{rq}}{dt} + \omega_r.\varphi_{rd} \end{cases} \quad (10)$$

$$\begin{cases} \varphi_{sd} = L_s.I_{sd} + M.I_{rd} \\ \varphi_{sq} = L_s.I_{sq} + M.I_{rq} \\ \varphi_{rd} = L_r.I_{rd} + M.I_{sd} \\ \varphi_{rq} = L_r.I_{rq} + M.I_{sd} \end{cases} \quad (11)$$

V_{sd}, V_{sq}, V_{rd} and V_{rq} are respectively the voltages of the stator and rotor; I_{sd}, I_{sq}, I_{rd} and I_{rq} represent the currents of the stator and rotor; R_s and R_r represent respectively the stator and rotor windings resistances; L_s, L_r and M are respectively the inductance on the stator, the inductance on the rotor and the mutual inductance; w_s represent the stator electrical pulsation and w_r is the rotor one. These pulsations are linked by the following expression:

$$w_r = w_s - w \quad (12)$$

It is possible to express the electromagnetic torque of the DFIG as a function of the currents and fluxes as follows:

$$C_{em} = p.\left(\varphi_{sd}.I_{sq} - \varphi_{sq}.I_{sd}\right) \quad (13)$$

p is the DFIG's number of pole pairs.

The stator active and reactive powers generated by the DFIG stator are expressed as:

$$\begin{cases} P_s = V_{sd}.I_{sd} + V_{sq}.I_{sq} \\ Q_s = V_{sq}.I_{sd} - V_{sd}.I_{sq} \end{cases} \quad (14)$$

The rotor side converter is controlled in a Park frame synchronized with the flux vector of the stator, which aligned on the d-axis (Fig.9) [14]. The stator resistance is neglected and the grid is considered stable and perfect. Consequently:

$$\varphi_{sd} = \varphi_s,\ \varphi_{sq} = 0,\ V_{sd} = 0 \text{ and } V_{sq} = V_s = \omega_s.\varphi_s$$

Using the previous assumptions, the rotor voltages and the stator powers can be written as demonstrate in Eq. (15).

σ is the dispersion coefficient of Blondel and g is the slip of the DFIG.

$$\begin{cases} V_{rd} = R_r.I_{rd} + \dfrac{dI_{rd}}{dt} - g.\omega_s.L_r.\sigma.I_{rq} \\ V_{rq} = R_r.I_{rq} + \dfrac{dI_{rq}}{dt} + g.\omega_s.L_r.\sigma.I_{rd} + g\dfrac{M.V_s}{L_s} \\ P_s = -\dfrac{V_s}{L_s}M.I_{rq} \\ Q_s = \dfrac{V_s^2}{\omega_s.L_s} - \dfrac{V_s}{L_s}M.I_{rd} \end{cases} \quad (15)$$

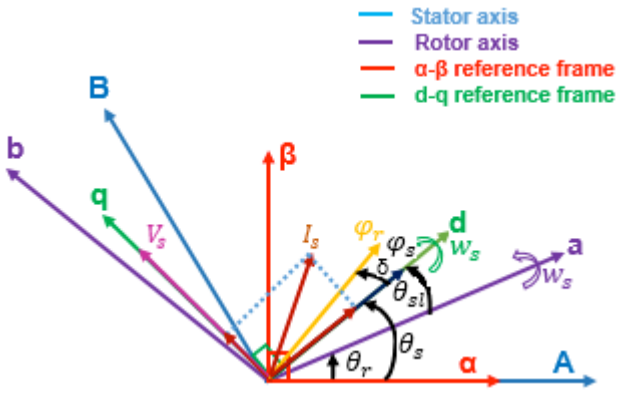

Fig. 9. Field oriented control strategy

By using Eq. (13), the electromagnetic torque is expressed in the following relation:

$$C_{em} = -p\frac{M.\varphi_s}{L_s}\cdot I_{rq} \quad (16)$$

The block diagram of a simplified model of the DFIG is presented in Fig.10.

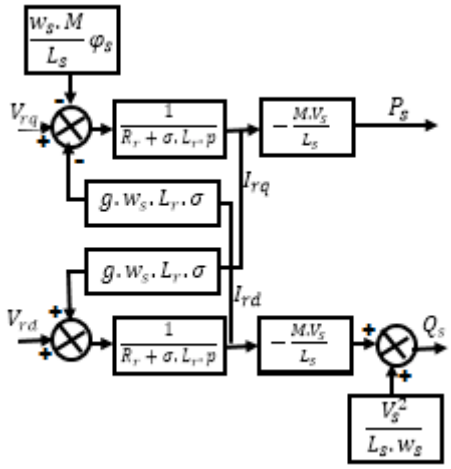

Fig. 10. Simplified model of the DFIG

5. Vector Control of DFIG

5.1. Direct Vector Control (DVC)

The direct vector control (DVC) consists to neglecting the terms of coupling between the two axes (d and q), an independent controller on each axis is introduced to regulate individually the stator active and reactive powers. This control is called direct control because the powers controllers regulate directly the rotor voltages of the DFIG, as we see in Fig.11.

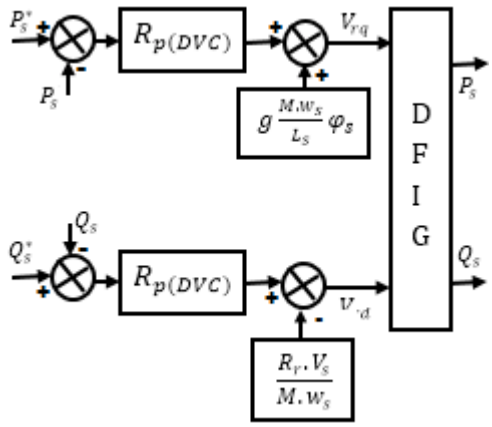

Fig. 11. DVC control schemes of the DFIG stator powers

5.2. Indirect Vector Control (IVC)

The indirect vector control (IVC) takes into account the coupling terms between d-q axes. Therefore, a vector control with two regulators per each axis is obtained as shown in Fig.12.

The open loop transfer functions of stator powers $F_{P_s(Q_s)}$ and rotor currents $F_{I_{rd}(I_{rq})}$ are given as:

$$F_{P_s(Q_s)}(s) = \frac{M.V_s}{\sigma.L_s.L_r.s + L_s.R_r}\ ,\quad F_{I_{rd}(I_{rq})}(s) = \frac{1}{\sigma.L_r.s + R_r}$$

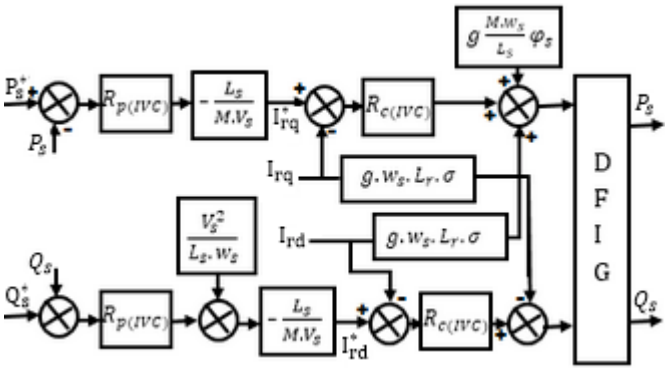

Fig. 12. IVC control schemes of the DFIG stator powers

6. Sliding Mode Control Principle and Application

In this last two decades, the sliding mode control has known a great success for robust control of the nonlinear system. This is due to its robustness against the uncertainties of the system and the external perturbations (sudden speed variations); and also to its simple implementation compared to the other types of controllers [20].

The basic idea of SMC technique is to attract the system state vector toward the sliding surface, then the system slides on this surface to the desired equilibrium point.

To define the sliding surface, the fundamental equation proposed by J. J. Slotine is taken [11, 20]:

$$S(X) = \left(\frac{d}{dt} + \lambda\right)^{n-1}.e(X) \tag{17}$$

$e = X^* - X$ is the error, n is relative degree and λ is a positive coefficient.

The active and reactive powers of the stator are linked respectively to quadrature rotor current and direct rotor current. The error signals between the references and measured rotor currents are presented in the following relation:

$$\begin{cases} e_d = I_{rd}^* - I_{rd} \\ e_q = I_{rq}^* - I_{rq} \end{cases} \tag{18}$$

To control the stator powers, $n = 1$ has been taken; consequently, the sliding surfaces illustrating the error signals between the references and the measured currents of the rotor can be given as follows:

$$\begin{cases} \dot{S}(I_{rd}) = \dot{I}_{rd}^* - \frac{1}{L_r.\sigma}\left(V_{rd} - R_r.I_{rd} + g.w_s.\sigma.L_r.I_{rq}\right) \\ \dot{S}(I_{rq}) = \dot{I}_{rq}^* - \frac{1}{L_r.\sigma}\left(V_{rq} - R_r.I_{rq} - g.w_s.\frac{M.\varphi_s}{L_s} - g.W_sL_r.\sigma.I_{rd}\right) \end{cases} \tag{19}$$

The control law V_{ri} is composed of two parts, V_{ri-eq} represents the equivalent part of the control and V_{ri-n} is the discontinuous part:

$$V_{ri} = V_{ri-eq} + V_{ri-n} \tag{20}$$

Where: i represent the direct (d) and quadrature (q) frame axes.

During the steady state and the sliding mode, the sliding surface becomes zero, so its derivative and the discontinuous control become zero. Therefore, the equivalent controls can be deduced as given in the following relation:

$$\begin{cases} V_{rd-eq} = L_r.\sigma.\dot{I}_{rd}^{*} + R_r.I_{rd} - g.w_s.L_r.\sigma.I_{rq} \\ V_{rq-eq} = L_r.\sigma.\dot{I}_{rq}^{*} + R_r.I_{rq} + g.w_s.L_r.\sigma.I_{rd} + g\dfrac{M.V_s}{L_s} \end{cases} \quad (21)$$

The condition of convergence is defined by using the general equation proposed by Lyapunov. This condition keeps the surface attractive and invariant.

$$\begin{cases} S(I_{rd}).\dot{S}(I_{rd}) < 0 \\ S(I_{rq}).\dot{S}(I_{rq}) < 0 \end{cases} \quad (22)$$

The simplest form used to represent the discontinuous part is a relay. Therefore, the discontinuous parts are given by Eq. (23):

$$\begin{cases} V_{rd-n} = K_d.sign\left(S(I_{rd})\right), \ K_d > 0 \\ V_{rq-n} = K_q.sign\left(S(I_{rq})\right), \ K_q > 0 \end{cases} \quad (23)$$

The sliding phase corresponds to that of a relay (Eq. (23)) switching with an infinite frequency. An infinite oscillation frequency assumes ideal switching elements, which doesn't exist in practice. In the presence of these imperfections, the switching frequency becomes finite and is manifested by oscillations around the sliding surface S. These oscillations have a greater amplitude and a lower frequency. This phenomenon is called a "chattering phenomenon". To avoid this problem, which can even destroy the equipment of the system, the discontinuous function "sign" is replaced by the continuous one [11]; which represents the saturation function in our case as shown in Eq. (24).

$$\begin{cases} V_{rd-n} = K_d.\mathrm{Sat}\left(S(I_{rd})\right), \ K_d > 0 \\ V_{rq-n} = K_q.\mathrm{Sat}\left(S(I_{rq})\right), \ K_q > 0 \end{cases} \quad (24)$$

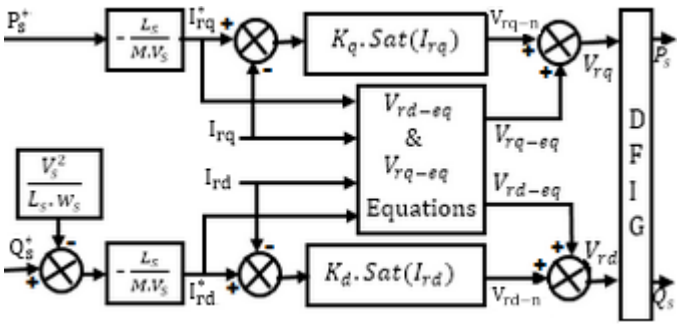

Fig. 13. The Block diagram of a stator powers control by using SMC

The block diagram of proposed SMC control technique, which is presented and designed to independently regulate the stator active and reactive powers of the DFIG, is illustrated in Fig.13.

7. Simulation Results and Discussions

In this section, the simulation results are carried out with a 7.5 kW machine attached to a perfect and stable grid 400 V/50 Hz using MATLAB/Simulink software. The overall system parameters studied are summarized in Table 1 and Table 2 presented in the appendix. The both control techniques, PI (DVC and IVC) and SMC, are simulated and compared regarding stator powers reference tracking, sensitivity to perturbations (rotor speed variations) and robustness against DFIG parameter variations.

7.1. Reference tracking

The aim of this first test is to investigate the behavior of the two control techniques, PI and SMC, while the speed of the machine is set at its nominal value (300 rad / s). As shown in Fig.14, Fig.15, Fig.16 and Fig.17, the active and reactive powers of a stator, the rotor active power and electromagnetic torque follow their reference values but with an important response time for the DVC compared to the IVC and SMC.

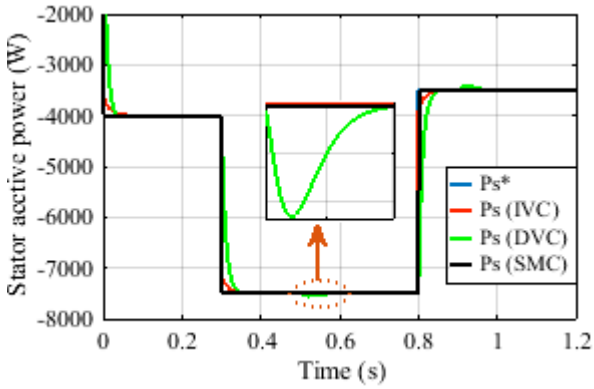

Fig. 14. P_s **:** PI (DVC and IVC) and SMC strategies responses (reference tracking test).

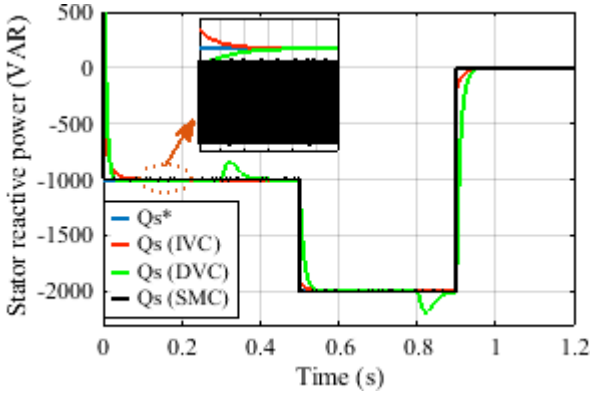

Fig. 15. Q_s **:** PI (DVC and IVC) and SMC strategies responses (reference tracking test).

The stator active power is always kept negative, this is mean that the DFIG operates as a generator; however, the

rotor active power is positive, which means that the rotor is a receiver of the energy supplied by the grid. Hence, the DFIG operates as a hypo-synchronous generator. We can also note that the electromagnetic torque (Fig.17) depends directly on the stator active power P_s, this is translated by its identical form to that of the P_s (Fig.14). In this case, we can conclude that the active power is a consequence of the electromagnetic torque.

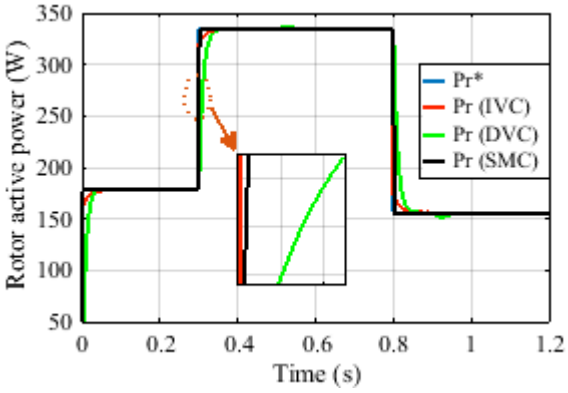

Fig. 16. P_r : PI (DVC and IVC) and SMC strategies responses (reference tracking test).

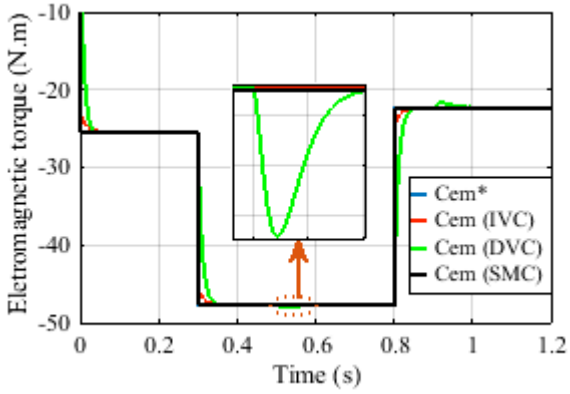

Fig. 17. C_{em} : PI (DVC and IVC) and SMC strategies responses (reference tracking test).

Using the conventional PI controllers especially the direct vector control (DVC), the coupling effect between the both stator active and reactive powers of the DFIG was observed. While the indirect vector control (IVC) and sliding mode control (SMC) guarantee the decoupling between them.

7.2. Sensibility to perturbations (mechanical speed variation)

The aim of this second test is to evaluate the impact of rotor speed variation on stator active and reactive powers for both control techniques, PI and SMC. For this, the rotational speed of the DFIG was varied in the time interval t = 0 s to t = 1.2 s as shown in Fig.18.

The simulation results are shown in Fig.19 and Fig.20. From these figures, we can observe that the mechanical speed variation introduces a remarkable effect on stator active and reactive powers curves for PI controllers especially the DVC. While the SMC shows its robustness by rejecting the effects of disturbances.

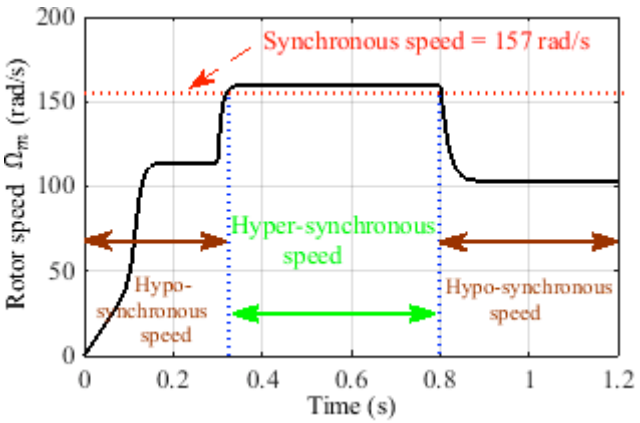

Fig. 18. Mechanical speed of the DFIG

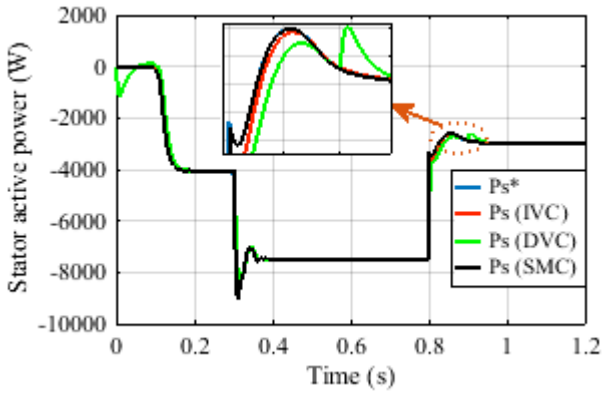

Fig. 19. P_s : PI and SMC strategies responses (sensitivity to the rotor speed variation)

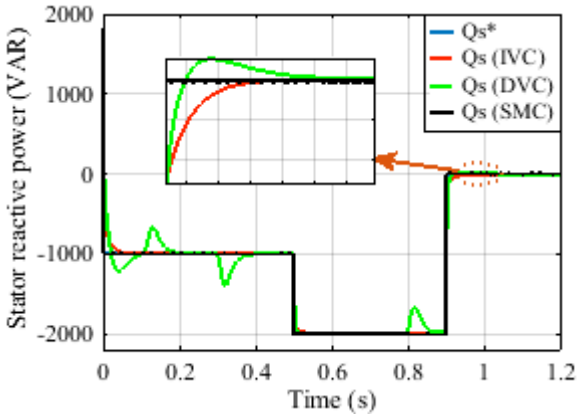

Fig. 20. Q_s : PI and SMC strategies responses (sensitivity to the rotor speed variation)

The stator active power is limited to its nominal value (7.5 KW) by using the pitch angle control to protect the WTS from overloading when the speed of wind exceeds the nominal one. The currents of the stator and rotor are presented in Fig.21 and Fig.22. The rotor currents are sinusoidal and present a low frequency (f_r) that satisfies the relation $f_r = g.f_s$.

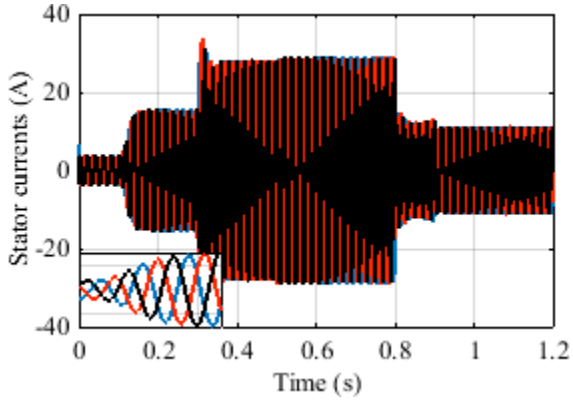

Fig. 21. The stator currents (sensitivity to the rotor speed variation)

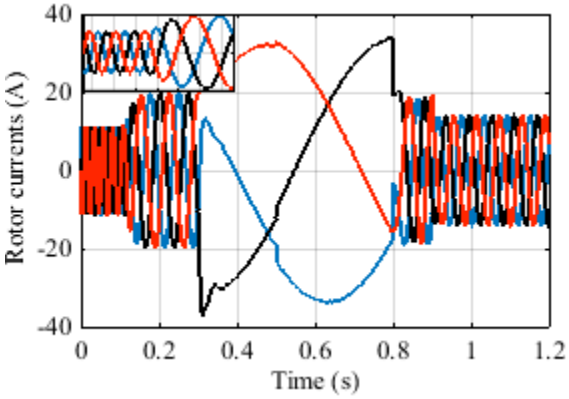

Fig. 22. The rotor currents (sensitivity to the rotor speed variation)

7.3. Robustness test (sensibility to the parameters variation)

The robustness of both controllers (PI and SMC) used in our case is an important point, especially for systems with several interacting entities or those with large variations of parameters. In this test, the DFIG is running at its rated speed (300 rad / s).

Firstly, the value of the rotor resistance is doubled. The simulation results are shown in Fig.23, Fig.24, Fig.25 and Fig.26. Secondly, the values of inductances L_s, L_r and M are divided by 2; the simulation results are presented in Fig.27, Fig.28, Fig.29 and Fig.30.

As shown in these figures, the effect of perturbation appears clearly at the stator powers in the case of PI controllers and especially for DVC. This is due to two reasons: the first is that we find only one control loop on currents and powers; the second is that the term $\frac{g.M.V_s}{L_s}$ on the q-axis represents an electromotive force depends on the rotation speed, which its influence is not neglected because it causes an error between the reference and measured value. The rotor resistance variation increases the response time of the stator powers, while the variation of inductances values affects the dynamic and static performance of DVC and IVC. Consequently, these variations introduce a clear impact on the stator powers curves in term of response time and static error as shown in Fig.27 and Fig.28. This effect appears more significant for PI controllers than for SMC one.

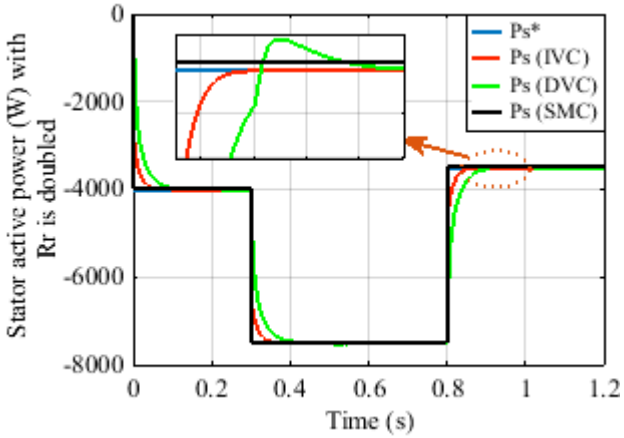

Fig. 23. P_s : PI and SMC strategies responses (robustness test - variation of resistance).

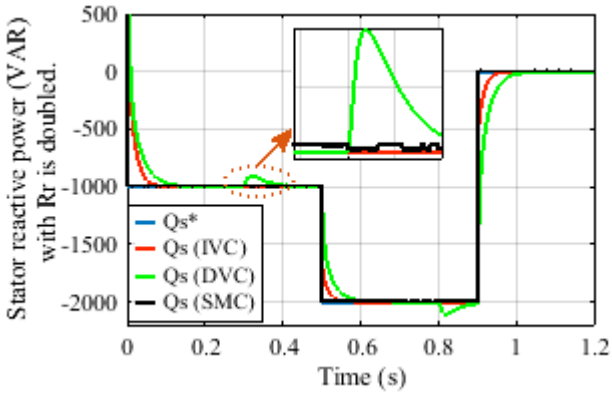

Fig. 24. Q_s : PI and SMC strategies responses (robustness test - variation of resistance)

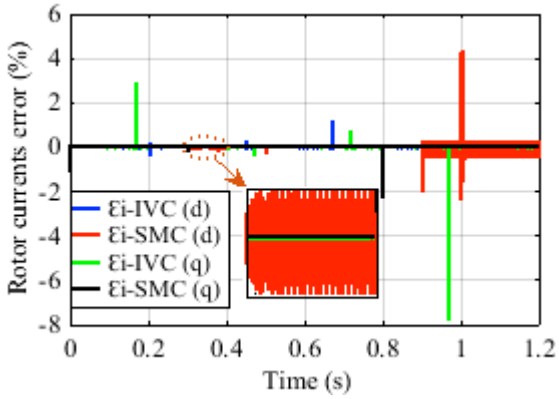

Fig. 25. Rotor current error curves (robustness test - variation of resistance)

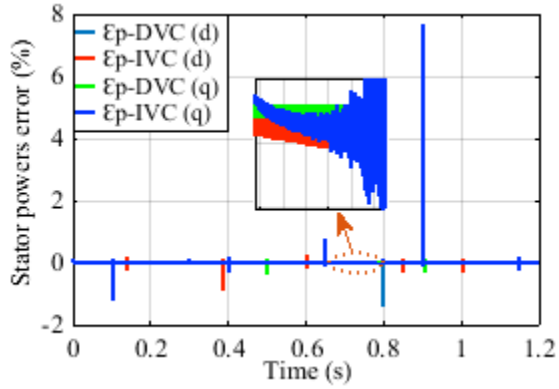

Fig. 26. Stator power error curves (robustness test - variation of resistance)

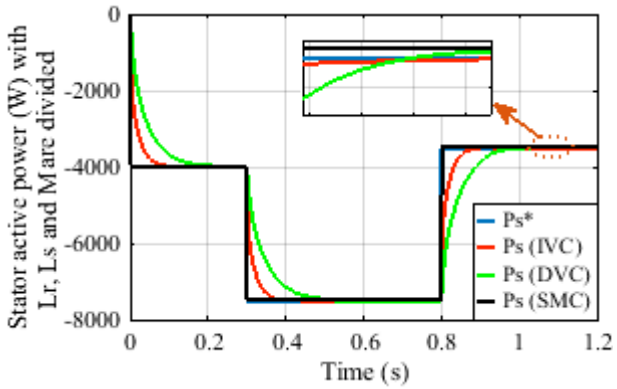

Fig. 27. P_s : PI and SMC strategies responses (robustness test - variation of inductances)

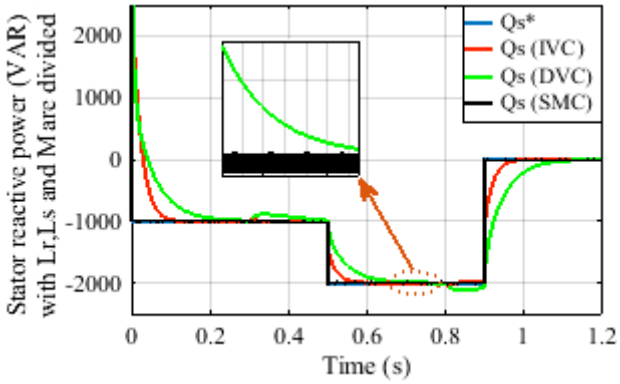

Fig. 28. Q_s : PI and SMC strategies responses (robustness test - variation of inductances)

From the simulation results and the static errors obtained for each control strategy, the proposed SMC strategy present a fast dynamic response with a negligible static error. The SMC strategy presents good results regarding the decoupling between the two axes d-q, consequently the decoupling between the stator powers. Therefore, it can be concluded that the proposed SMC control technique is more robust against the variations of mechanical speed and sensitivity to parameters variations than the PI one.

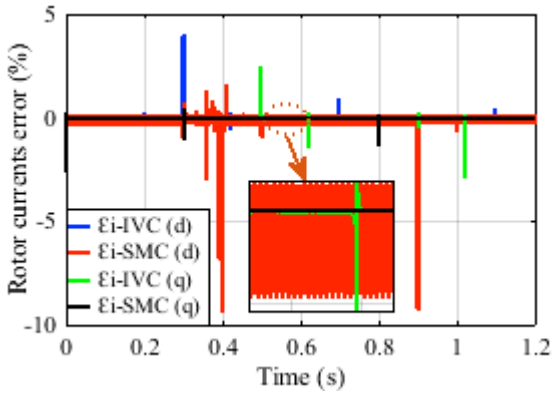

Fig. 29. Rotor current error curves (robustness test - variation of inductances)

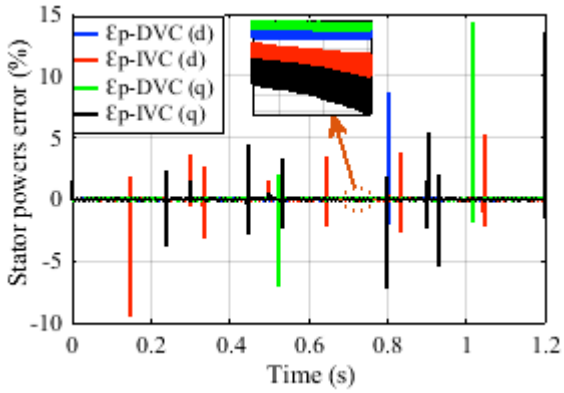

Fig. 30. Stator power error curves (robustness test - variation of inductances).

8. Conclusion

The PI and robust SMC control strategies of stator active and reactive powers have been presented in this paper. The DFIG is integrated into a WECS and connected directly to the electrical grid by its stator, while its rotor side connected to the electrical grid via two converters. The uses of a DFIG in WTS offers several advantages, such as variable speed operation, reduction of the inverter cost and its capability of operation in four quadrants. The MPPT and pitch angle control strategies are used in this simulation to improve the performances of the WECS. As a first step, the modeling of the turbine and DFIG is carried out in order to apply the stator field orientation technique.

In the second step, the PI and SMC controllers were presented and synthesized in order to independently control the stator powers. The measured powers track their references for both controllers, but a coupling effect appears clearly in the case of PI (DVC and IVC) responses, which is removed in the case of SMC one. When the DFIG's rotational speed is changed, the impact of perturbation is more remarkable on the stator powers for PI strategy, and especially for DVC, compared to SMC one. The effect of DFIG parameters variation has also been examined. These changes affect the dynamic and permanent regimes of active and reactive powers responses, but with an important effect with PI strategy compared to that with SMC. The simulation results have confirmed that the proposed SMC present fast

dynamic responses with negligible steady state error. All these results prove that a robust SMC strategy can be considered as a very interesting solution for WECS using DFIG.

Appendix

Table 1. DFIG and Wind turbine parameters

DFIG Parameters	
Nominal power	7.5 Kw
Number of pairs poles p	2
Rated stator voltage V_s	220 V
Stator frequency f_s	50 Hz
Stator resistance R_s	0.45 Ω
Rotor resistance R_r	0.62 Ω
Stator inductance L_s	0.084 H
Rotor inductance L_r	0.081 H
Mutual inductance M	0.078 H
Moment of inertia J	0.043 $Kg.m^2$
Friction coefficient f	0.017 $N.m.s/rad$
Wind turbine Parameters	
Blade number	3
Blade radius R	4 m
Gearbox gain G	5.4
Maximum power coefficient $C_{p-\max}$	0.4745
Optimum tip-speed ratio λ_{cp-opt}	8.16

Table 2. Different WECS commands parameters

Systems	**Parameters**	**Value**
PI (MPPT with control of speed)	K_p K_i	25.8 7899
PI (Pitch angle control)	K_p K_i	29.4 441
PI- $R_p(DVC)$ (Direct Vector control)	K_p (power) K_i (power)	0.00419 0.30034
PI- $R_p(IVC)$ & Rc (IVC) (Indirect Vector control)	K_p (power) K_i (power) K_p (current) K_i (current)	0.00419 0.30034 8.5698 620
Sliding mode control (SMC)	Gain K_d Gain K_q	2000 1000

Acknowledgements

This work has been supported by National Center for Scientific and Technical Research (CNRST), Rabat, Morocco.

References

[1] I. Colak, G. Fulli, S. Bayhan, S. Chondrogiannis, S. Demirbas "Critical aspects of wind energy systems in smart grid applications", Renewable and Sustainable Energy Reviews, ScienceDirect, DOI: 10.1016/j. rser.2015.07.062, Vol. 52, pp. 155-171, December 2015. (Article)

[2] X. Zhao, D. Luo, "Driving force of rising renewable energy in China: Environment, regulation and employment", Renewable and Sustainable Energy Reviews, vol. 68, pp. 48-56, September 2016. (Article)

[3] Z. Boudjema, R. Taleb, Y. Djeriri, and A. Yahdou, "A novel direct torque control using second order continuous sliding mode of a doubly fed induction generator for a wind energy conversion system", Turkish. J. Elec. Eng. Comp. Sci, vol. 25, pp. 965-975, April 2017. (Article)

[4] R. Chakib, A. Essadki, and T. Nasser, "Active Disturbance Rejection Control for Wind System Based On a DFIG", International Journal of Electrical, Computer, Energetic, Electronic and Communication Engineering, vol. 8, No. 8, pp. 1306-1315, 2014. (Article)

[5] A. Bakouri, A. Abbou, H. Mahmoudi, K. Elyaalaoui, "Direct Torque Control of a Doubly Fed Induction Generator of Wind Turbine for Maximum Power Extraction", IEEE, International Renewable and Sustainable Energy Conference (IRSEC), Ouarzazate, Morocco, pp. 334-339, 17-19 October 2014. (Conference paper)

[6] A. Elmansouri, J. El mhamdi, A. Boualouch, "Wind Energy Conversion System Using DFIG Controlled by Back-stepping and RST Controller", IEEE, 2nd International Conference on Electrical and Information Technologies ICETT'2016, Tangiers, Morocco, pp. 312-318, 4-7 May 2016. (Conference paper)

[7] F. Poitiers, T. Bouaouiche, M. Machmoum "Advanced control of a doubly-fed induction generator for wind

energy conversion", Electric Power Systems Research, ScienceDirect, Vol. 79, pp. 1085-1096, July 2009. (Article)

[8] T. Ghennam, Supervision d'une ferme éolienne pour son intégration dans la gestion d'un réseau électrique, Apports des convertisseurs multi niveaux au réglage des éoliennes à base de machine asynchrone à double alimentation, No. 162. September 2011. (Book)

[9] V. Utkin, H. Lee, "Chattering Problem in Sliding Mode Control Systems", Proceedings of the 2006 International Workshop on Variable Structure Systems Alghero, Italy, 5-7 June 2006. (Conference paper)

[10] I. Bendaas, F. Naceri, "A New Method to Minimize the Chattering Phenomenon in Sliding Mode Control Based on Intelligent Control for Induction Motor Drives", SERBIAN Journal of Electrical Engineering, vol. 10, No. 2, pp. 231-246, June 2013. (Article)

[11] A. Attou, A. Massoum., and E. Chiali, "Sliding mode control of a permanent magnets synchronous machine", 4th International Conference on Power Engineering, Energy and Electrical drives, Istanbul, 13-17 May 2013. (Conference paper)

[12] A. Boukhriss, T. Nasser, and A. Essadki, "A Linear Active Disturbance Rejection Control applied for DFIG based Wind Energy Conversion System", International Journal of Computer Science Issues, vol. 10, pp. 391-399, March 2013. (Article)

[13] M. Allam, B. Dehiba, M. Abid, and Y. Djeriri, " Etude comparative entre la commande vectorielle directe et indirecte de la Machine Asynchrone à Double Alimentation (MADA) dédiée à une application éolienne", Journal of Advanced Research in Science & Technology, ISSN. 2352-9989, June 2014. (Article)

[14] C. Mehdipou, A. Hajizadech, I. Mahdipour, "Dynamic modeling and control of DFIG-based wind turbines under balanced network conditions", Electrical Power and Energy Systems, ScienceDirect DOI: 10.1016/j.ijepes.2016.04.046, Vol. 83, pp. 560-569, April 2016. (Article)

[15] I. Nouira, and A. Khedher, "A Contribution to the Design and the Installation of an Universal Platform of a Wind Emulator using a DC Motor", International Journal of Renewable Energy Research, vol. 2, pp. 797-804, October 2012. (Article)

[16] S. El Aimani, Modélisation des différentes technologies d'éoliennes intégrées dans un réseau de moyenne tension, No. 4. December 2004. (Book)

[17] A. Dahbi, N. Nait-Said, M. S. Nait-Said, "A novel combined MPPT-pitch angle control for wide range variable speed wind turbine based on neural network", International Journal of Hydrogen Energy, ScienceDirect, DOI: 10.1016/j.ijhydene.2016.03.105, Vol. 41, Issue. 22, pp. 9427-9442, June 2016. (Article)

[18] S. Kahla, Y. Soufi, M. Sedraoui, M. Bechouat, "On-Off control based particle swarm optimization for maximum power point tracking of wind turbine equipped by DFIG connected to the grid with energy storage", International Journal of Hydrogen Energy, ScienceDirect, DOI: 10.1016/j.ijhydene.2015.05.007, Vol. 40, Issue. 39, pp. 13749-13758, October 2015. (Article)

[19] A. Bakouri, A. Abbou, H. Mahmoudi, and K. Elyaalaoui, "Direct Torque Control of a Doubly Fed Induction Generator of Wind Turbine for Maximum Power Extraction", IEEE International Renewable and Sustainable Energy Conference, Morocco. New York, pp. 334-339, 17-19 October 2014. (Conference paper)

[20] A. Mechter, K. Kemih, and M. Ghanes, "Sliding Mode Control of a Wind Turbine with Exponential Reaching Law", Acta Polytechnica Hungaria, vol. 12, No. 3, pp. 167-183, 2015. (Article)